batteries

MDPI

Article

First Principles Study of the Phase Stability, the Li Ionic Diffusion, and the Conductivity of the $Li_{10}Ge_xMo_{1-x}P_2S_{12}$ of Superionic Conductors

Yifang Wu [1], Yuanzhen Chen [2] and Shaokun Chong [3,*]

[1] Northwest Institute for Nonferrous Metal Research, Xi'an 710016, China; wyf7777v@126.com
[2] State Key Laboratory for Mechanical Behavior of Materials, School of Materials Science and Engineering, Xi'an Jiaotong University, Xi'an 710049, China; cyz1984@xjtu.edu.cn
[3] Frontiers Science Center for Flexible Electronics, Institute of Flexible Electronics, Northwestern Polytechnical University, Xi'an 710072, China
* Correspondence: iamskchong@nwpu.edu.cn

Abstract: Using first-principles density functional theory (DFT) calculations and ab initio molecular dynamics (AIMD) simulations, we performed this study on the phase stability, the intrinsic redox stability, and the Li^+ conductivity of $Li_{10}Ge_xMo_{1-x}P_2S_{12}$ (x = 0~1) superionic conductors. Molybdenum (Mo) is expected to replace expensive germanium (Ge) to lower tmaterial costs, reduce sensitivity to ambient water and oxygen, and achieve acceptable Li^+ conductivity. The ab initio first principle molecular dynamics simulations show that room-temperature Li^+ conductivity is 1.12 $mS{\cdot}cm^{-1}$ for the $Li_{10}Ge_{0.75}Mo_{0.25}P_2S_{12}$ compound, which is comparable to the theoretical value of 6.81 $mS{\cdot}cm^{-1}$ and the experimental measured one of 12 $mS{\cdot}cm^{-1}$ of the $Li_{10}GeP_2S_{12}$ (LGPS) structure. For $Li_{10}Ge_xMo_{1-x}P_2S_{12}$ (x = 0, 0.25, 0.5 and 1) compounds, the density of states and the projection fractional wave state density were calculated. It was found that when Ge atoms were partially replaced by Mo atoms, the band gap remained unchanged at 2.5 eV, but deep level defects appeared in Mo-substituted compounds. Fortunately, this deep level defect is difficult to ionize at room temperature, so it has no effect on the electronic conductivity of Mo substitute compounds, making Mo substitution a suitable solution for electrolyte materials. The projection fractional wave state density calculation shows that the covalent bond between Mo and S is stronger than that between Ge and S, which reduces the sensitivity of Mo-substituted compounds to water and oxygen contents in the air. In addition, the partial state density coincidence curve between Li and S elements disappears in the 25% Mo-substituted compound with energies of 4–5 eV, indicating that the Li_2S by-product is decreased.

Keywords: first principles; ab initio molecular dynamics; superionic conductors; solid electrolytes; lithium-ion battery

Citation: Wu, Y.; Chen, Y.; Chong, S. First Principles Study of the Phase Stability, the Li Ionic Diffusion, and the Conductivity of the $Li_{10}Ge_xMo_{1-x}P_2S_{12}$ of Superionic Conductors. *Batteries* **2024**, *10*, 344. https://doi.org/10.3390/batteries10100344

Academic Editor: Seokheun Choi

Received: 22 August 2024
Revised: 21 September 2024
Accepted: 26 September 2024
Published: 27 September 2024

1. Introduction

Lithium-ion batteries (LIBs) have experienced rapid development in the past decade and are widely used in various fields such as medicine, aerospace, and power storage [1]. More stringent criteria for electrolyte materials have been put in place due to the ongoing push for high performance lithium-ion batteries [2]. The highest Li^+ conductivity ever recorded has been found in the $Li_{10}GeP_2S_{12}$ (LGPS) superionic conductor among solid lithium electrolytes, which has the conductivity of 12 $mS{\cdot}cm^{-1}$ at room temperature [3–6].

Despite its cutting-edge Li^+ conductivity and high electrochemical performance, the use of LGPS as a solid electrolyte material is still hindered by three significant issues. First, there is the practical problem of using highly expensive and scarce germanium in LGPS, which would prevent the widespread usage of the substance. Second, the air and moisture sensitivity of sulfide-based compounds can make their manufacture and application more

expensive. Third, lithium metal is too prone to chemically react with sulfur elements in LGPS through reduction reactions and generate Li_2S by-products [7].

Researchers have developed a number of strategies to improve the air/water stability of LGPS, including isovalent cation substitutions of Ge^{4+} by Si and Sn and aliovalent cation substitutions by Al [8]. These substituting strategies mainly involve substituting with elements of the same group as Ge or elements adjacent to Ge in the periodic table. However, these elements are hard acids, which is hard to bond with the soft base of S. According to Hard and Soft Acid and Bases (HSAB) theory [9,10], hard acids and bases generally have smaller radii and polarizabilities than soft acids and bases. Hard acids and hard bases are preferentially bound mainly by coulomb forces, while soft acids and soft bases are preferentially bound mainly by covalent bonds. To date, the use of soft acids as substituting elements has not been reported in the literature. Soft acids are substances that can easily accept electron pairs, usually with high polarizability and easily deformable electron orbitals, but have a weak polarization to distort the electron cloud of other atoms or ions. Soft acids include a series of metal ions such as Cu^+, Cu^{2+}, Ag^+, Cd^{2+}, Hg^{2+}, Au^+, Au^{3+}, Pt^{2+}, Pd^{2+}, Mo^{2+}, and Mo^{4+}, etc. The softer acid Mo^{4+} was specially chosen in this work because isovalent cation substitution is expected to have a small effect on the phase stability, electrochemical stability, and lithium-ion diffusivity as for LGPS. Based on HSAB theory, S is a softer base than O and prefers to bind with soft acids such as Mo^{2+} and Mo^{4+}. Therefore, Mo-element substitution in LGPS could not only reduce the material cost but also effectively mitigate the erosion of O in the air, thus helping to maintain the good electrochemical properties of superionic conductors.

In this work, we investigate the phase stability, intrinsic redox stability, and Li^+ conductivity of $Li_{10}Ge_xMo_{1-x}P_2S_{12}$ (x = 0~1) superionic conductors using first principle calculations. Our aim was to search for an effective element substitution with a similar structural makeup to LGPS, which can strike a better balance between electrochemical performance, cost, and other features.

2. Computational Details

The Vienna Ab initio Simulation Package (VASP) and the projector augmented-wave (PAW) method were used for all calculations in this work. Considering the accuracy and computational cost of different requirements in this paper, we have carefully chosen the suitable functionals and methods for each technique as listed in the following sections.

2.1. Modeling and Structure Optimization

Due to the co-occupation of the Li#1-4, Ge#1, and P#1 atoms in the $Li_{10}GeP_2S_{12}$ (LGPS) structure, it is difficult to conduct simulation calculations. Hence, it was a heavy task to convert a co-occupancy model to full occupancy ones. Eventually, sixty-one full occupancy $Li_{20}Ge_2P_4S_{24}$ models were constructed to identify which atoms fit in which spots. Similarly, sixty-one full occupancy $Li_{20}Mo_2P_4S_{24}$ models were constructed. The PBE generalized-gradient approximation (GGA) functional was employed by DFT calculations to find out the lowest energy of various $Li_{20}Ge_2P_4S_{24}$ and $Li_{20}Mo_2P_4S_{24}$ models to obtain optimized relaxation structures. Structure substitution models for the partial substitution of Mo, namely the $Li_{20}GeMoP_4S_{24}$ model and the $Li_{40}Ge_3MoP_8S_{48}$ supercell model, were implemented on the $Li_{20}Ge_2P_4S_{24}$ model with the lowest energy structure. After Mo substitution, optimal relaxation structures were still obtained using the DFT calculation.

2.2. Binding Energy

When we design a new material through element substitution, the first thing we need to do is to determine whether the material is stable, which is a very key link in the field of material design.

Binding energy refers to the energy released by atoms from their free state to form compounds. For a simple binary compound A_mB_n (where A and B are the two elements

contained in the compound, and m and n are the number of corresponding atoms in the chemical formula), its binding energy can be calculated according to the following formula:

$$E_b = \frac{\mathrm{E}(\mathrm{A}_m\mathrm{B}_n) - \mathrm{m} \times \mathrm{E}(\mathrm{A}) - \mathrm{n} \times \mathrm{E}(\mathrm{B})}{\mathrm{m} + \mathrm{n}} \quad (1)$$

where $\mathrm{E}(\mathrm{A}_m\mathrm{B}_n)$ is the ground-state energy of $\mathrm{A}_m\mathrm{B}_n$, and E(A) and E(B) are the energies of free atoms A and B, respectively. All of these energies are calculated in units of eV (electron volts). The more negative the value of E_b, the more stable it is.

In this paper, the PBE generalized-gradient approximation (GGA) functional was employed by DFT calculations to evaluate ground-state energies of various $Li_{10}Ge_xMo_{1-x}P_2S_{12}$ (x = 0~1) models and free energies of Li, Ge, Mo, P, and S single atoms.

2.3. Intrinsic Redox Stability

By figuring out the material's band gap, we evaluated the $Li_{10}Ge_xMo_{1-x}P_2S_{12}$ (x = 0~1) solid electrolyte's inherent stability with regard to inert electrodes. Due to the substantial underestimation of band gaps by standard semi-local DFT, the density of states (DOS) of $Li_{10}Ge_xMo_{1-x}P_2S_{12}$ (x = 0~1) compounds were calculated using the Heyd–Scuseria–Ernzerhof (HSE06) screened hybrid functional [11], which has been tested to give relatively accurate band gaps for a wide range of materials [12,13].

Non-spin-polarized calculations were carried out since $Li_{10}Ge_xMo_{1-x}P_2S_{12}$ compounds do not contain 3D transition metal ions (V to Ni) or other atoms with f-shell outer electrons. The bandgap is not a precise indicator of the electrochemical stability on inert electrodes because it is unknown how it aligns to an external reference potential. However, it might be viewed as the upper limit of the electrochemical window [14].

2.4. Lithium-Ion Transport Capabilities

Using ab initio molecular dynamics (AIMD) simulations, we evaluated the Li^+ diffusivity and conductivity in $Li_{10}Ge_xMo_{1-x}P_2S_{12}$ (x = 0~1) compounds. The Brillouin zone was precisely integrated in the reciprocal space using the γ-point scheme with $3 \times 3 \times 2$ k-meshes. The generalized gradient approximation (GGA) parametrized by Perdew, Burke, and Ernzerhof (PBE) was employed for the exchange−correlation functional, and the PBE configured projected-augmented wave (PAW) method was applied to describe interactions among core electrons. Plane wave basis functions for the Kohn−Sham equation were reduced to an energy cutoff of 259 eV to keep the computing cost at a manageable level. All calculations were performed using a non-spin-polarized. The Verlet algorithm was employed in VASP to integrate Newton's equation. The molecular dynamics time step was set as 2 fs. The AIMD simulations were performed as follows:

1. The $Li_{10}Ge_xMo_{1-x}P_2S_{12}$ (x = 0~1) samples are assigned an initial temperature of 100 K based on a Boltzmann distribution at the start of the MD simulations.
2. The samples are then heated to the required temperature (600 to 1200 K) by velocity scaling over 1000 time steps (2 ps) in the NVT ensemble with a constant volume and a Nosé–Hoover thermostat, and then equilibrated at the equilibrium temperature for 5000 time steps (10 ps) in the NVT ensemble with a constant volume and a Nosé–Hoover thermostat.
3. The MD simulations for diffusion are then run in the NVT ensemble for 40 ps to 100 ps until the diffusion coefficient converges.

To get the diffusion coefficient D, the mean square displacements are utilized over time:

$$D = \frac{1}{2dt}\left\langle [r(t)]^2 \right\rangle \quad (2)$$

where d equals 3, the dimension of the lattice in which diffusion occurs. The t refers to time, counted in unit of fs. The average mean square displacement $\left\langle [r(t)]^2 \right\rangle$ was determined as follows:

$$\left\langle [r(t)]^2 \right\rangle = \frac{1}{N}\sum_i \left\langle \left[r_i(t+t_o)^2 \right] - [r_i(t_o)]^2 \right\rangle \quad (3)$$

where $r_i(t)$ represents the displacement of the i-th Li ion at time t. The calculated displacement $r_i(t)$ represents the displacement of a single Li atom, calculated in the unit of Å. The diffusion coefficient D is determined in $Å^2 \cdot fs^{-1}$ and can be converted to $cm^2 \cdot s^{-1}$ by a multiple of 10^{-1}.

The Nernst–Einstein relation was used to calculate the Li ionic conductivity σ in units of $mS \cdot cm^{-1}$.

$$\sigma = D\frac{\rho Z^2 F^2}{RT} \quad (4)$$

where D is the diffusion coefficient of Li ions in units of $cm^2 \cdot s^{-1}$ in a unit cell. The ρ, Z, F, R, and T are the molar density in units of mol/L, the mean valence electronic charge of a Li ion (dimensionless), the Faraday constant in units of KJ/(V·mol), the gas constant in units of J/(mol·K), and the absolute temperature, respectively.

The Arrhenius equation was used to calculate the average diffusion activation energy of lithium ion E_a in units of eV.

$$\sigma = A \cdot exp\left(-\frac{E_a}{kT}\right) \quad (5)$$

where σ is the Li ionic conductivity. A represents predigital factor. E_a, k, and T are the average diffusion activation energy of lithium ion, the Boltzmann constant in units of eV/K, and the absolute temperature, respectively.

3. Results and Discussion

3.1. Relaxed Structural and Parameters

The optimal relaxation structures of the $Li_{10}Ge_xMo_{1-x}P_2S_{12}$ (x = 0~1) models are shown in Figure 1, in which Figure 1a–d correspond to the $Li_{20}Ge_2P_4S_{24}$, $Li_{20}GeMoP_4S_{24}$, $Li_{40}Ge_3MoP_8S_{48}$, and $Li_{20}Mo_2P_4S_{24}$ structures, respectively. The changes in lattice parameters after Mo substitution are shown in Table 1. For comparison, for the $Li_{40}Ge_3MoP_8S_{48}$ model, both the c-axis lattice parameter and the cell volume are divided by 2.

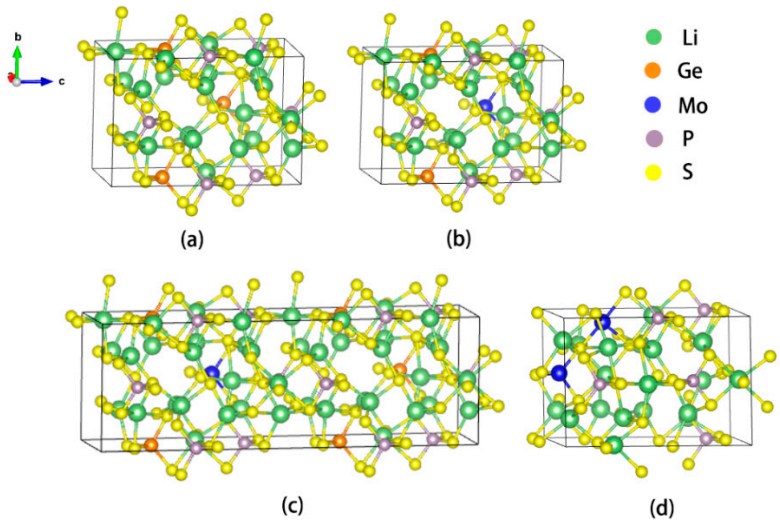

Figure 1. The optimal relaxation structures of $Li_{10}Ge_xMo_{1-x}P_2S_{12}$ (x = 0~1) models. (**a**) $Li_{20}Ge_2P_4S_{24}$, (**b**) $Li_{20}GeMoP_4S_{24}$, (**c**) $Li_{40}Ge_3MoP_8S_{48}$, and (**d**) $Li_{20}Mo_2P_4S_{24}$.

Table 1. The lattice parameters of relaxed $Li_{10}Ge_xMo_{1-x}P_2S_{12}$ (x = 0~1) models.

	$Li_{20}Ge_2P_4S_{24}$	$Li_{40}Ge_3MoP_8S_{48}$	$Li_{20}GeMoP_4S_{24}$	$Li_{20}Mo_2P_4S_{24}$
a (Å)	8.6025	8.5905	8.5899	8.7922
b (Å)	8.6489	8.6606	8.6735	8.6187
c (Å)	12.8824	12.9232	12.9114	12.5916
α	89.1560	89.0088	88.9790	90.9771
β	90.2020	90.2727	90.3518	90.5599
γ	89.2361	89.1494	89.1528	89.6798
V (Å3)	958.2773	961.2006	961.6789	953.9658

3.2. Phase Stability

The binding energies of $Li_{10}Ge_xMo_{1-x}P_2S_{12}$ (x = 0~1) compounds are shown in Table 2. It shows that when the amount of Mo substitution grows, the binding energy becomes more and more negative, indicating improved phase stability.

Table 2. The binding energies of $Li_{10}Ge_xMo_{1-x}P_2S_{12}$ (x = 0~1) compounds.

	$Li_{20}Ge_2P_4S_{24}$	$Li_{40}Ge_3MoP_8S_{48}$	$Li_{20}GeMoP_4S_{24}$	$Li_{20}Mo_2P_4S_{24}$
binding energy (eV)	−4.29	−4.34	−4.39	−4.50

3.3. Bandgaps and Intrinsic Redox Stability

We estimated the density of states (DOS) of all $Li_{10}Ge_xMo_{1-x}P_2S_{12}$ (x = 0~1) compounds using the HSE screened hybrid functional (HSE06) to analyze the intrinsic redox stability of the various $Li_{10}Ge_xMo_{1-x}P_2S_{12}$ (x = 0~1) compounds. The calculated DOS for $Li_{10}Ge_xMo_{1-x}P_2S_{12}$ (x = 0~1) compounds are shown in Figure 2. Figure 2 indicates that bandgaps remain unchanged as Ge atoms are partially substituted by Mo, but the defect state energy level appears in Mo-substituted compounds. These defect state energy levels are located in the center of the forbidden band, far from the bottom of the conduction band or the top of the valence band, which belong to deep level defects. They are difficult to ionize at room temperature and do not affect the electronic conductivity of Mo-substituted compounds.

In $Li_{10}Ge_xMo_{1-x}P_2S_{12}$ (x = 0.5 and 0.75) crystal structures, the Mo atoms are adjacent to S atoms. The degree of coincidence of *DOS* between Mo and S elements near bandgaps at an energy of 1–2 eV are higher than that between Ge and S elements, indicating stronger binding forces between Mo and S elements, which is in accordance with the HSAB theory [15,16]. It can be seen from the projected DOS in the inset of Figure 2b at an energy of 1–2 eV that the binding energy between Mo and S is mainly contributed by the d orbital of Mo and the p orbital of S. Furthermore, it is noteworthy that for the $Li_{10}Ge_xMo_{1-x}P_2S_{12}$ (x = 0.75) compound, the coincidence curve of the partial wave state density between Li and S elements disappears when reaching an energy of 4~5 eV, indicating a decreased probability of forming Li_2S decomposition products of this compound.

The DOS results predict that the bandgap of $Li_{10}GeP_2S_{12}$ is about 2.5 eV, which would be sufficient for preventing electrical conduction. It suggests that the observed electrochemical window of >5 V for this material is likely the result of a passivation phenomenon, where either Li_2S or P_2S_5 is formed as a decomposition product [8]. As can be seen from Figure 2, the positions of the conduction band and the valence band of the Mo-substituted compounds shift down. This leads to an increase in the reduction potential of the compound and a decrease in the oxidation potential, which usually means that these electrolytes remain stable over a wider potential range, thereby improving the electrochemical stability of these electrolytes.

For 0.25 and 0.5 Mo-substituted compounds, bandgaps maintain unchanged except that medium-depth deep-level defects are induced. Generally, the ionization energy of medium-depth deep-level defects is usually between 0.1 eV and 0.5 eV. This energy range is sufficient to make the defect resistant to ionization at room temperature but can be

significantly ionized at higher temperatures, such as 100 °C to 300 °C. Obviously, even for batteries at elevated temperatures, which is far less than 100 °C, medium-depth deep-level defects in Mo-substituted compounds would have no impact on electronic conductivities of batteries. By contrast, in the case of the compound with complete Mo-substitution, there is an obvious contraction of the bandgap to 2.0 eV around. Generally speaking, this bandgap is big enough not to become a potential leakage channel.

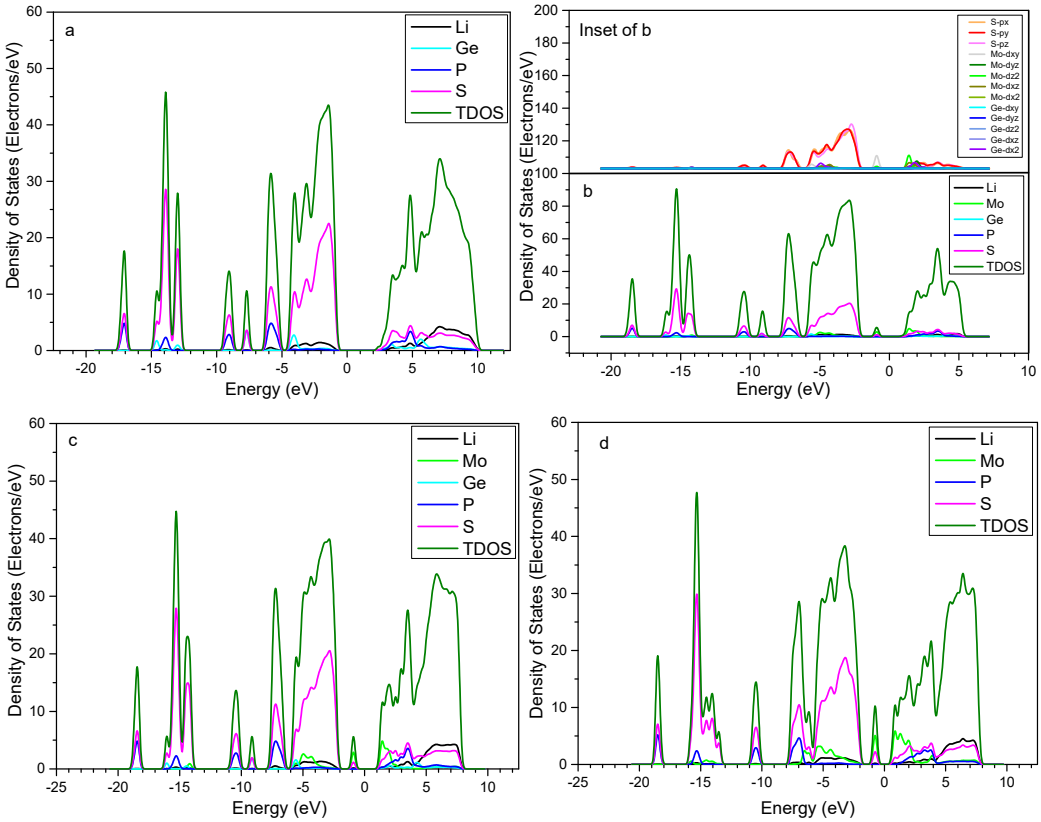

Figure 2. The calculated DOS for $Li_{10}Ge_xMo_{1-x}P_2S_{12}$ (x = 0~1) compounds. (**a**) $Li_{20}Ge_2P_4S_{24}$, (**b**) $Li_{40}Ge_3MoP_8S_{48}$, (**c**) $Li_{20}GeMoP_4S_{24}$, and (**d**) $Li_{20}Mo_2P_4S_{24}$. In all plots, the Fermi level is set to 0 eV and is marked by the dashed line. Inset of b is the projected DOS of the $Li_{40}Ge_3MoP_8S_{48}$ Compound.

3.4. Li^+ Diffusivity and Conductivity

Li ionic diffusion coefficients in $Li_{10}Ge_xMo_{1-x}P_2S_{12}$ (x = 0~1) crystal structures were determined by random walk theory and AIMD simulations as a function of T (=600, 800, 1000, and 1200 K) by vaspkit software 1.3.5 [17], as shown in Figure 3. The lithium-ion diffusion coefficients at room temperature (300 K) were calculated by the linear fitting extrapolation method in Figure 3.

The conductivities and diffusion activation energies of lithium ions were determined by the Nernst equation (See Equation (4)) and Arrhenius equation (See Equation (5)), respectively. The calculated Li ionic diffusion coefficients, conductivities, and diffusion activation energies of lithium ion in $Li_{10}Ge_xMo_{1-x}P_2S_{12}$ (x = 0~1) crystal structures are listed in Table 3. It demonstrates that when Ge is replaced by 25% Mo, lithium-ion conductivity still maintains 1.12 $mS{\cdot}cm^{-1}$, which is in the same order of magnitude as the theoretical predicted value of 6.81 $mS{\cdot}cm^{-1}$ in the LGPS structure (the experimental measured value is 12 $mS{\cdot}cm^{-1}$). The value of 6.81 $mS{\cdot}cm^{-1}$ is very similar to the calculated 6.43 $mS{\cdot}cm^{-1}$ in the recent reference [18]. As a result, appropriate Mo substitution can significantly cut raw material costs while just marginally lowering material conductivity.

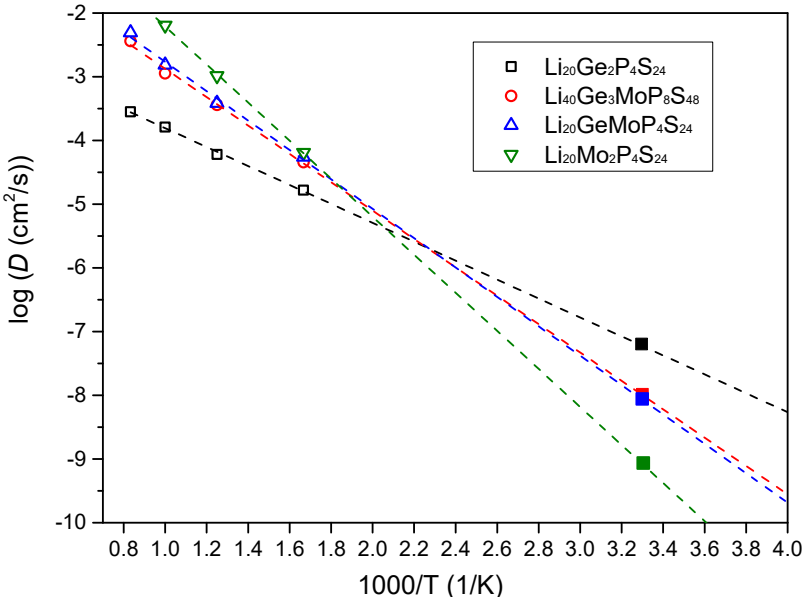

Figure 3. The Li ionic diffusion coefficients in $Li_{10}Ge_xMo_{1-x}P_2S_{12}$ (x = 0~1) crystal structures. The filled black square corresponds to the linearly extrapolated (dashed line) conductivity at 300 K from high-temperature conductivity.

Table 3. The calculated Li ionic diffusion coefficient, conductivity, and diffusion activation energy of lithium ion in $Li_{10}Ge_xMo_{1-x}P_2S_{12}$ (x = 0~1) crystal structures.

	Li Ionic Diffusion Coefficients ($cm^2 \cdot s^{-1}$)	**Conductivities of Lithium Ions ($mS \cdot cm^{-1}$)**	**Diffusion Activation Energies of Lithium Ions (eV)**
$Li_{20}Ge_2P_4S_{24}$	5.26×10^{-8}	6.81	0.23
$Li_{40}Ge_3MoP_8S_{48}$	8.66×10^{-9}	1.12	0.37
$Li_{20}GeMoP_4S_{24}$	7.13×10^{-9}	0.92	0.39
$Li_{20}Mo_2P_4S_{24}$	6.65×10^{-10}	0.09	0.53

The calculated activation energy of Li^+ diffusion for totally Mo-substituted $Li_{20}Mo_2P_4S_{24}$ (LMPS) of 0.53 eV is much greater than the 0.23 eV of LGPS, which fits in well with the literature [3,19–21], indicating a much higher diffusion barrier. As a result, the Li^+ conductivity at 300 K is only 0.09 $mS \cdot cm^{-1}$ for LMPS, which is two orders of magnitude lower than LGPS. For compounds with 0.25 and 0.5 Mo substitutes for Ge, calculated activation energies of Li^+ diffusion are between the values of LGPS and LMPS, indicating moderate diffusion barriers.

In fact, for compounds with 0.25 and 0.5 Mo substitutes for Ge, the diffusion of lithium ions remains in the 1D channel along the c-axis, supplemented by a-b plane diffusion pathways [20] because the crystal structure of these compounds does not change compared with LGPS. For these two compounds, their cell volumes are slightly increased, as shown in Table 1, which is favorable for the diffusion of lithium ions as indicated by the literature [8]. However, the diffusion channel of Li ions in these crystals may gradually shrink by an increased amount of Mo due to a higher atomic radius of Mo than Ge. There is an obvious contraction in the cell volume for the compound that Ge is completely replaced by Mo as shown in Table 1, which would lead to a severely constricted lithium-ion diffusion channel and an enormous decrease in the conductivity of lithium ions as indicated in Table 3.

3.5. Discussion

By executing Mo substitutions to create $Li_{10}Ge_xMo_{1-x}P_2S_{12}$ (x = 0~1) compounds, we investigated the characteristics that influence structural, phase, and redox stability and Li ionic diffusivity.

For 0.25 and 0.5 Mo-substituted compounds, their cell volumes are slightly increased while crystal structures remain unchanged. In contrast, there is a distinct contraction in the cell volume for the compound with 100% Mo-substitution.

Our calculation demonstrates that as the content of Mo substitution grows in $Li_{10}Ge_x Mo_{1-x}P_2S_{12}$ (x = 0~1) compounds, the binding energy becomes increasingly negative, indicating increased phase stability.

In terms of redox stability, the calculated DOS suggests that the redox stability remains unchanged for $Li_{10}Ge_xMo_{1-x}P_2S_{12}$ (x = 0.5 and 0.75) compounds. The shift down of calculated conduction bands and valence bands indicates an increase in the reduction potential of the compound and a decrease in the oxidation potential, which means a larger stable electrochemical window. However, when reaching complete Mo-substitution, the bandgap starts to contract, indicating a decline in the inherent redox stability of the compound.

Additionally, the coincidence curve of the partial wave state density between the Li and S elements vanishes at an energy of 4~5 eV for the 0.25 Mo-substituted compound, indicating the decreased probability of forming the Li_2S decomposition product of this compound.

The LMPS compound has a two-orders-of-magnitude lower diffusivity than the LGPS compound, which makes it significantly less interesting than LGPS. This decrease in diffusivity in the LMPS compound is most likely due to the significantly reduced cell volume. The calculated activation energy of Li^+ diffusion for LMPS of 0.53 eV is also significantly higher than 0.23 eV of LGPS.

By contrast, $Li_{10}Ge_{0.5}Mo_{0.5}P_2S_{12}$ and $Li_{10}Ge_{0.75}Mo_{0.25}P_2S_{12}$ compounds have slightly increased cell volume. Hence, higher conductivities of lithium ions are anticipated in these two compounds, which are also projected to lower the cost of raw materials. Our calculation shows that the preferred substitution rate for Ge by Mo is less than 25%. At this rate, lithium-ion conductivity remains at 1.12 $mS{\cdot}cm^{-1}$, which is worthy of comparison with the calculated value of 6.81 $mS{\cdot}cm^{-1}$ of the LGPS structure. The activation energy of the compound is also only 0.14 eV higher than that of LGPS.

In general, for the solid-state synthesis of LGPS, the synthetic raw materials are Li_2S, P_2S_5, and GeS_2. When partial Mo substitution for Ge is adopted, it is relatively easy in synthesis as long as the stoichiometric ratio is well controlled and part of the GeS_2 in the raw materials is replaced by MoS_2. Only by reducing the cost of materials and improving the chemical stability and electrochemical stability of materials, can the large-scale application of new materials be achieved.

4. Conclusions

The necessity to address three key constraints of the LGPS superionic conductor, namely the expensive cost of germanium, the air and moisture sensitivity of a sulfide-based chemistry, and the reduction reaction tendency of lithium metal with sulfur elements, have spurred our exploration of Mo-substituted $Li_{10}Ge_xMo_{1-x}P_2S_{12}$ (x = 0~1) compounds.

Our calculations show that the substitution of 0.25 Mo for Ge is the optimal choice for compounds with this structure, which not only lowers the material cost by adding an appropriate amount of Mo but also reduces the sensitivity of the compound to water and oxygen in the air by improving the binding force between Mo and S, with improved electrochemical stability and suppressed Li_2S by-products. But all of these are at the expense of a slightly decreased conductivity of lithium ions at 1.12 $mS{\cdot}cm^{-1}$ for this compound, which is comparable to the predicted value of 6.81 $mS{\cdot}cm^{-1}$ for the LGPS structure.

The calculated DOS show that bandgaps remain unchanged as Ge atom are partially substituted by Mo, however, the deep defect state energy level appears in these compounds. Fortunately, it is difficult to ionize at ambient temperature and make no impact on their electronic conductivities. The shift down of the conduction band and valence band of the partially Mo-substituted compounds leads to an increase in the reduction potential of the compound and a decrease in the oxidation potential, suggesting a wider potential range and an improved electrochemical stability of compounds.

In conclusion, we believe that replacing Ge with an appropriate Mo atom is an effective strategy to lower material cost and improve chemical stability and electrochemical stability. It is worth noting that the first-principles simulation can only give a theoretical guide, and exactly suitable Mo doping or substitution amounts need to be verified by subsequent experiments. However, theoretical simulations have demonstrated the feasibility of Mo substituting Ge in synthesis and large-scale applications.

Author Contributions: Methodology, Y.W.; Software, Y.C.; Formal analysis, Y.W.; Writing—original draft, Y.W.; Writing—review & editing, S.C.; Funding acquisition, Y.C. and S.C. All authors have read and agreed to the published version of the manuscript.

Funding: This work was supported by National Natural Science Foundation of China (52207248), Guangdong Basic and Applied Basic Research Foundation (2022A1515010208 and 2021A1515110164), and the Open Testing Foundation of Analytical & Testing Center of Northwestern Polytechnical University (2022T024), the Joint Funds of the Natural Science Basic Research Project of Shaanxi Province (No. 2021JLM-23), and the University Joint Project of Shaanxi Province (2021GXLH-Z-067).

Data Availability Statement: The raw data supporting the conclusions of this article will be made available by the authors on request.

Acknowledgments: The authors gratefully acknowledge the High Performance Computing of Network Information Center, Xi'an Jiaotong University for first-principles simulations.

Conflicts of Interest: The authors declare no conflict of interest.

References

1. Zhang, S.Y.; Gu, K.H.; Lu, B.A.; Han, J.W.; Zhou, J. Hydrometallurgical Processes on Recycling of Spent Lithium-Ion Battery Cathode: Advances and Applications in Sustainable Technologies. *Acta Phys.-Chim. Sin.* **2024**, *40*, 2309028. [CrossRef]
2. Zhang, J.K.; Lv, J.C.; Lu, W.; Li, X.; Liu, Y.; Lang, J.H.; Liu, J.; Wang, Z.; Lu, M.; Sun, H. $Li_{10}GeP_2S_{12}$-based solid electrolyte induced by high pressure for all-solid-state batteries: A facile strategy of low-grain-boundary-resistance. *Chem. Eng. J.* **2024**, *487*, 150452. [CrossRef]
3. Kamaya, N.; Homma, K.; Yamakawa, Y.; Hirayama, M.; Kanno, R.; Yonemura, M.; Kamiyama, T.; Kato, Y.; Hama, S.; Kawamoto, K.; et al. A lithium superionic conductor. *Nat. Mater.* **2011**, *10*, 682–686. [CrossRef] [PubMed]
4. Hwang, T.; Conlin, P.; Cho, M.; Cho, K. Electrochemical Stability and Li Ion Diffusion Kinetics of Grain Boundaries in $Li_{10}GeP_2S_{12}$ Solid Electrolyte. *J. Phys. Chem. C* **2023**, *127*, 7528–7535. [CrossRef]
5. Zhang, J.; Huang, L.; Gu, X. Failure mechanism of solid-state electrolyte $Li_{10}GeP_2S_{12}$ in a moist atmosphere: A first-principles study. *Mater. Adv.* **2022**, *3*, 3143–3150. [CrossRef]
6. Wang, Q.; Liu, D.; Ma, X.; Liu, Q.; Zhou, X.; Lei, Z. Sb-doped $Li_{10}GeP_2S_{12}$-type electrolyte $Li_{10}SnP_{2-x}Sb_xS_{12}$ with enhanced ionic conductivity and lower lithium-ion migration barrier. *J. Colloid Interface Sci.* **2022**, *627*, 1039–1046. [CrossRef]
7. Zhao, J.; Zhao, C.; Zhu, J.P.; Liu, X.S.; Yao, J.M.; Wang, B.; Dai, Q.S.; Wang, Z.F.; Chen, J.Z.; Jia, P.; et al. Size-Dependent Chemomechanical Failure of Sulfide Solid Electrolyte Particles during Electrochemical Reaction with Lithium. *Nano Lett.* **2022**, *22*, 411–418. [CrossRef]
8. Ong, S.P.; Mo, Y.F. William Davidson Richards, Lincoln Miara, Hyo Sug Leeb and Gerbrand Ceder. Phase stability, electrochemical stability and ionic conductivity of the (M=Ge, Si, Sn, Al or P, and X=O, S or Se) family of superionic conductors. *Energy Environ. Sci.* **2013**, *6*, 148–156. [CrossRef]
9. Sahu, G.; Lin, Z.; Liu, J.; Dudney, N.; Liang, C. Air-stable, high-conduction solid electrolytes of arsenic-substituted Li_4SnS_4. *Energy Environ. Sci.* **2014**, *7*, 1053–1058. [CrossRef]
10. Yang, M.; Chen, L.Q.; Li, H.; Wu, F. Air/Water Stability Problems and Solutions for Lithium Batteries. *Energy Mater. Adv.* **2022**, *2022*, 9842651.
11. Heyd, J.; Scuseria, G.E.; Ernzerhof, M. Hybrid functionals based on a screened Coulomb potential. *J. Chem. Phys.* **2006**, *124*, 219906, Erratum in *J. Chem. Phys.* **2003**, *118*, 8207–8215. [CrossRef]
12. Heyd, J.; Scuseria, G.E. Efficient hybrid density functional calculations in solids: Assessment of the Heyd-Scuseria-Ernzerhof screened Coulomb hybrid functional. *J. Chem. Phys.* **2004**, *121*, 1187–1192. [CrossRef] [PubMed]
13. Henderson, T.M.; Paier, J.; Scuseria, G.E. Accurate treatment of solids with the HSE screened hybrid. *Phys. Status Solidi B* **2011**, *248*, 767–774. [CrossRef]
14. Ong, S.P.; Andreussi, O.; Wu, Y.; Marzari, N.; Ceder, G. Electrochemical windows of room-temperature ionic liquids from molecular dynamics and density functional theory calculations. *Chem. Mater.* **2011**, *23*, 2979–2986. [CrossRef]
15. Jian, Y.; Huang, Z.; Xing, J.; Sun, L.; Liu, Y.; Gao, P. Phase stability, mechanical properties and electronic structures of TiAl binary compounds by first principles calculations. *Mater. Chem. Phys.* **2019**, *221*, 311–321. [CrossRef]

16. Yang, J.; Huang, J.; Ye, Z.; Fan, D.; Chen, S.; Zhao, Y. First-principles calculations on structural energetics of Cu-Ti binary system intermetallic compounds in Ag-Cu-Ti and Cu-Ni-Ti active filler metals. *Ceram. Int.* **2017**, *43*, 7751–7761. [CrossRef]
17. Wang, V.; Xu, N.; Liu, J.-C.; Tang, G.; Geng, W.-T. VASPKIT: A User-Friendly Interface Facilitating High-Throughput Computing and Analysis Using VASP Code. *Comput. Phys. Commun.* **2021**, *267*, 108033. [CrossRef]
18. Nachimuthu, S.; Cheng, H.-J.; Lai, H.-J.; Cheng, Y.-H.; Kuo, R.T.; Zeier, W.G.; Hwang, B.J.; Jiang, J.-C. First-principles study on selenium-doped $Li_{10}GeP_2S_{12}$ solid electrolyte: Effects of doping on moisture stability and Li-ion transport properties. *Mater. Today Chem.* **2022**, *26*, 101223. [CrossRef]
19. Kuhn, A.; Duppel, V.; Lotsch, B.V. Tetragonal $Li_{10}GeP_2S_{12}$ and Li_7GePS_8-exploring the Li ion dynamics in LGPS Li electrolytes. *Energy Environ. Sci.* **2013**, *6*, 3548–3552. [CrossRef]
20. Mo, Y.F.; Ong, S.P.; Ceder, G. First Principles Study of the $Li_{10}GeP_2S_{12}$ Lithium Super Ionic Conductor Material. *Chem. Mater.* **2012**, *24*, 15–17. [CrossRef]
21. Wang, Z.; Shao, G. Theoretical design of solid electrolytes with superb ionic conductivity: Alloying effect on Li^+ transportation in cubic Li6PA5X chalcogenides. *J. Mater. Chem. A* **2017**, *5*, 21846–21857. [CrossRef]